Int.J. Thermodynamics,
Vol.6 (No.1), pp.41-48, March-2003

ISSN 1301-9724

Analysis of Energy Conversion within a Radial Turbine Stage

G. DESCOMBES*, F. MAROTEAUX, N. MORENO, J. JULLIEN
Université P. et M. Curie,
Laboratoire de mécanique physique,
2, place de la gare de ceinture
78210 Saint Cyr l'école, France

Abstract

The results of a detailed study of energy conversion within a radial turbocharger turbine stage are presented in this paper. A 2.5D simulation is conducted near the optimum running point in order to construct the local aero thermodynamic flow field and the associated mechanical energy production within the rotor. Then, a complementary analysis of the flow led within each of the turbine sub-blocks is summarized. The simulation uses models of losses which are studied locally with a multi-dimensional approach and then reduced in 1D description (models reduction) allowing establishment of a global turbine performances map. The evaluation of losses appears to be particularly troublesome within such small machines. Losses due to flow-blade profile mismatch which represent a large source of energy dissipation are modeled by way of the entropy balance. The results are compared and validated in accordance with the experiments that were conducted on special turbocharger tests rigs and on a Diesel truck engine test bench.

Key words: *radial turbine, 2.5D analysis, mechanical energy production, energy conversion, incidence losses*

1. Introduction

The running conditions of a turbocharger turbine for road propulsion applications are very severe. The mass flow rate entering the turbine varies over a ratio of 1:5. The turbine can comprise a single or double volute, a smooth or vaned distributor the rotor remains of the helico-radial type to satisfy the engine performance requirements. This study aims at establishing the rotor permeability characteristics as a function of conditions at the turbine inlet in order to establish the performance of the complete turbocharger turbine. As a reminder, the turbines developed during the 1980's made use of a right-angle rotor blade inlet angle, a very marked deflection of the order of $\beta > 65°$ at rotor exit and a closed disk. The geometry of the rotor blade channels has since evolved towards a very compact open disk rotor configuration with more moderate exit angles ($\beta \approx 45°$) and curved blades in the axial plane. In the case of micro-turbines for 1000 cc Diesel engine applications, the rotor blade inlet remains at a right angle and closed disks are used due to the high centrifugal forces caused by rotation speeds approaching 250,000 rpm.

2. Aero and Thermodynamic Flow Description

Local mechanical energy production is analyzed by the pressure gradient present in the circumferential plane of the turbine rotor (*Figure 1*). The torque torsor associated with the relative movement expressed from velocity (Equation 1) and acceleration (Equation 2) composition laws gives a local view of the forces (Equation 3.a or Equation 3.b) and moments (Equation 4). The turbine shaft is at a steady regime, P is the static pressure and *v* the elementary volume.

$$\vec{V} = \vec{U} + \vec{W} = \vec{\omega} \Lambda \vec{r} + \vec{W} \tag{1}$$

$$\frac{d\vec{V}}{dt} = \frac{\partial \vec{V}}{dt} + \vec{V}\vec{\nabla}\vec{V} \tag{2}$$

$$d\vec{F} = \left[\vec{W}\vec{\nabla}\vec{W}\right]dm + \left[2\vec{\omega}\Lambda\vec{W}\right]dm + \left(\vec{\omega}\Lambda\left[\vec{\omega}\Lambda\vec{r}\right]\right)dm \tag{3a}$$

$$d\vec{F} = -\vec{\nabla}P dv \tag{3b}$$

$$d\vec{M} = \vec{r}\Lambda d\vec{F} \tag{4}$$

* Author to whom all correspondence should be addressed.

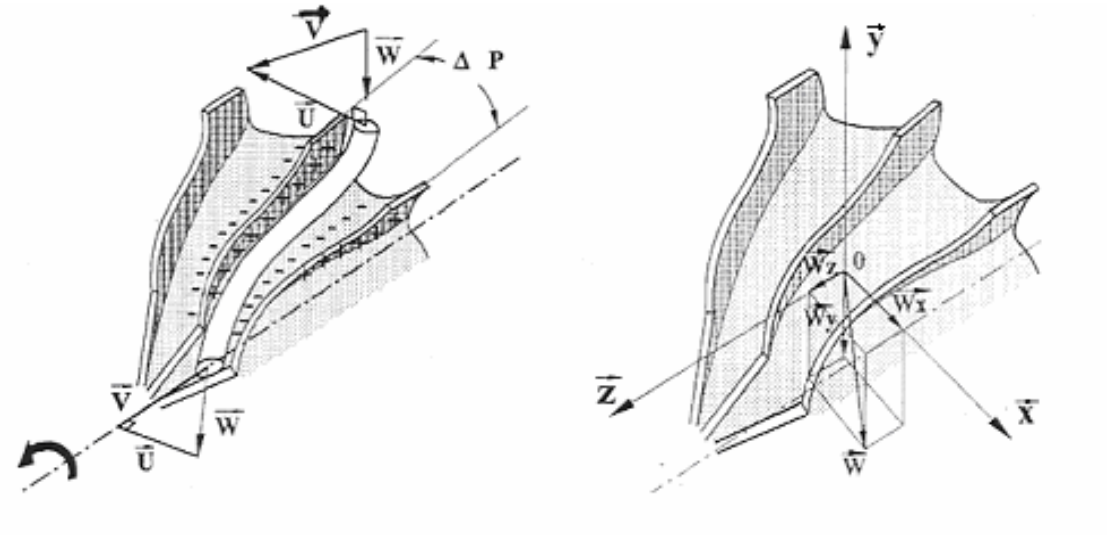

Figure 1. Gradient pressure and relative velocity within the rotor

Mechanical energy production is expressed according to the scalar moment of the rotor rotation (5) which expresses the respective variation of relative momentum $d(rW_x)$ and Coriolis momentum $d(\omega r^2)$. Both of these contribute to the energy conversion process within the helico-radial rotor. All of these equations are solved in the simulation to calculate the radial equilibrium and tangential momentum within circumferential and meridian planes.

$$\int_1^2 |dM_z| = \int_{A2} \left[r_2 W_{2x} + \omega r_2^2 \right] dq_m - \int_{A1} \left[r_1 W_{1x} + \omega r_1^2 \right] dq_m \qquad (5)$$

3. 2.5D Simulation

3.1 Concept

Experimental analysis, Descombes et al (1998), indicates that the distributions of velocity vectors and pressure scalars show marked gradients as a function of curvature radius and trajectory. Furthermore, this phenomenon represents a source of losses which remain difficult to model. The 2.5D simulation aims at establishing first of all the flow description in the meridian (S2) and circumferential (S1) planes of the machine (*Figure 2*) following the concept established by Wu (1951). The numerical scheme is based on the velocity potential function and assumed that the axi-symmetric flow has no rotating secondary movement (no swirl) within the mobile channel. This hypothesis means that the inlet and outlet planes of the rotor are perpendicular to the meridian streamlines.

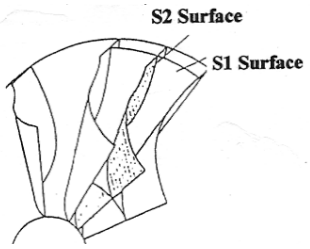

Figure 2. (S1) and (S2) surfaces in the rotor

3.2 Geometry modeling

The distributor is smooth and the rotor geometry undergoes a detailed metrology and numerical analysis in order to establish the profile of the channel between blades. The flow is assumed axi-symmetric, steady of an inviscid incompressible gas in the meridian plane and an inviscid compressible gas in the circumferential plane. The mesh machine uses a curvilinear and variable step scheme with 10000 nodes. *Figure 3* and *4* illustrate the meridian and circumferencial machine which is modeled by an inlet and fixed smooth distributor (1), the rotor (2) and an outlet and fixed diffuser (3).

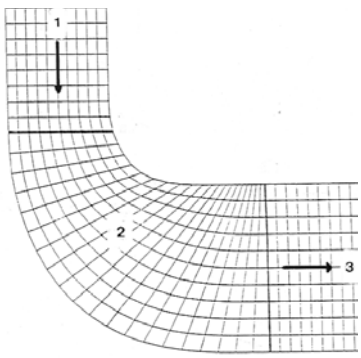

Figure 3. Schematic of the mesh in the S2 plane

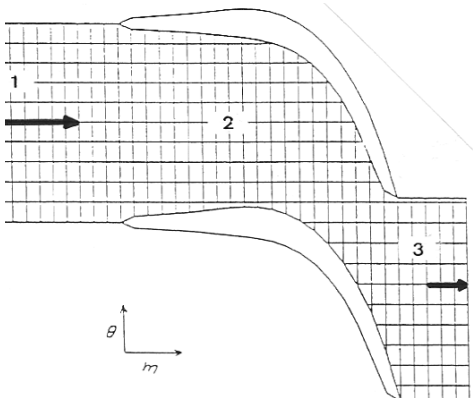

Figure 4. Schematics of the mesh in the S1 plane

4. Results

The turbine inlet conditions have been tested on a large range of thermodynamics values and several incidence angle conditions at the rotor blade inlet. We present here some results corresponding to the experimental data of Toussaint et al. 1999, around the optimum running point tested on a specific turbocharger test bed at cold condition flow. The experimental values are N_t=43020 rpm, q_m=0,79 kg.s^{-1}, P_i=130500 Pa, T_i=300 K.

4.1 Aero and thermodynamic distribution.

Figure 5 shows the mesh geometry of nine meridian streamlines. The indices 1, 2 and 3 identify the inlet distributor 1, the rotor 2 and the exhaust diffuser 3. One notes that the stream-tube close to the hub has a highly deformed profile due to flow deceleration at the blade channel walls which satisfies the uniform flow rate condition within each stream tube. *Figure 6* shows the validated distribution of the speed in the turbine as a function of meridian abscissa for five meridian lines from the hub to the top of the rotor.

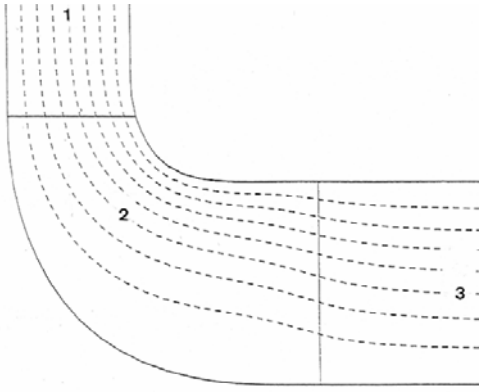

Figure 5. Schematics of the meridian streamlines

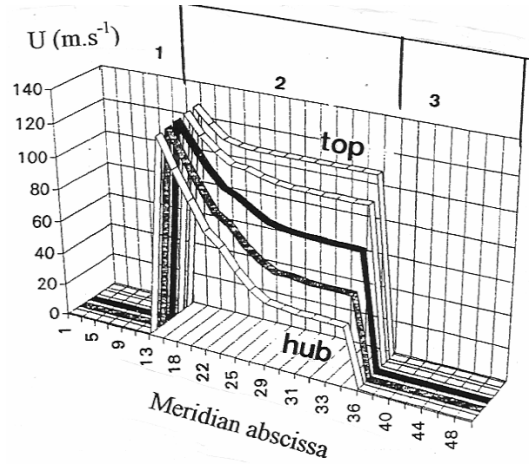

Figure 6. Meridian velocities at five lines

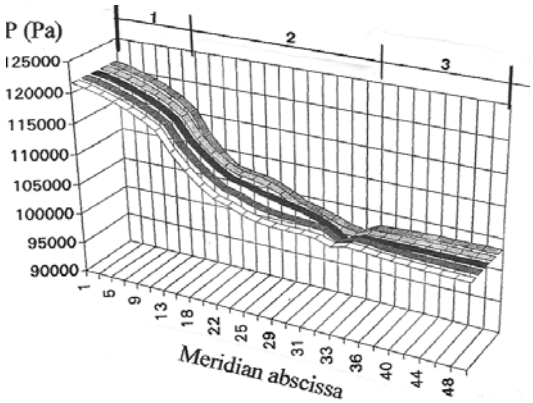

Figure 7. Relative static pressure at five lines

Figure 7 shows the static pressure P in the meridian plane and we observe a standard decrease of these values within the mobile and absolute description. *Figures 8* and *9* show the absolute velocity V and the relative velocity W in the meridian plane for the approximately zero incidence condition. It comes as no surprise to see a steady decrease in absolute velocity V and an increase in relative velocity W in the transverse plane from the hub to the outer radius.

We can see on the pressure and the velocities plots a peak near the hub of the rotor exit which has no physical meaning in the transversal plane. this peak expresses a numerical discontinuity between the relative and absolute description.

The calculation of the incidence flux profile deviation at the outlet rotor is based on the Kutta-Joukowski velocity equality condition at the channel trailing edge. This condition becomes difficult to follow in the near vicinity of the hub in this numerical scheme which is based on the resolution of the velocity potential equation.

The very small rotor radius in this region generates an unstability in the iterative

calculation of the partial radius derivatives, which locally tend towards very high values when the radius " r " tends towards zero (relation 1 in the velocity potential equation). This can generate local instabilities in the (r , z) meridian plane which disappear as soon as the curvature radius increases in the transverse plane.

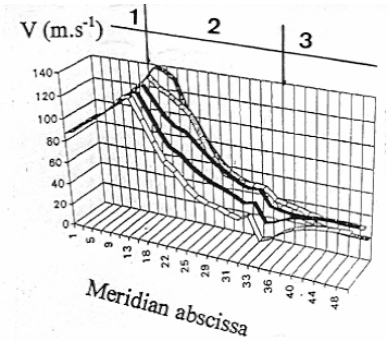

Figure 8. Absolute velocities at five lines

We note also that the curvilinear mesh channel is not adaptive enough around the exit hub of the blade geometry. This scheme can not of course restore any rotating secondary movement and it is unable to give convenient results outside of the optimum running point fixed near the zero incidence angle rotor blade inlet (Descombes 1997).

Implicit calculation schemes based on a complete resolution of the Navier equations in viscous fluids are now widely used, however the above method is still of interest in the vicinity of an adapted incidence point in an expansion machine.

We can note that another calculation has been led to compare the kinematic field computed in the meridian plane along a meridian line as a function of the incidence angle at the rotor inlet. The results are correct within the desadaptation range (-5 to 5°). Outside this range, the computation becomes wrong as mentioned above.

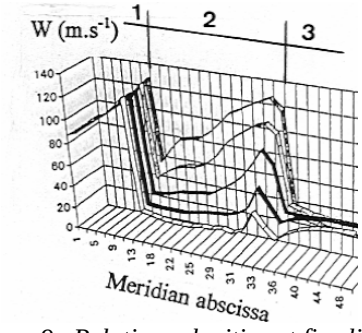

Figure 9. Relative velocities at five lines

4.2 Mechanical energy production

Figures 10 and *11* show the changes in relative and absolute tangential velocity which are directly responsible for the mechanical energy production on the shaft as equation (5). These results are in agreement with the local study within the next detailed simulation led within the rotor; for example for the experimental point: at 43020 rpm (constant speed line), with a flow rate equal to 79 g/s and an expansion ratio equal to 1.26 for an adaptative incidence condition. The power calculated at the outlet mean radius (r_m =1/2 (r_{max}+r_{min})$^{1/2}$ is equal to 1443 W, which corresponds to an exchanged work per unit mass of 18265 J/kg. The calculated power from the integrated values obtained from the 2.5D model on the outlet radius (EULER approach) is equal to 1394 W (-3,36%) and to 1380 W when we only take into account the friction losses (-4,37%).

The rotor is then divided into three distinct zones, which correspond respectively to the radial inlet 1, the helico-centripetal channel 2 between the blades and the axial rotor exit 3. The evolution of the transformation of a fluid particle is studied along the longitudinal and transverse trajectory in the meridian plane. TABLE I indicates the local and cumulative mechanical energy production within each rotor sub-block.

These results satisfy analytical checks imposed by the standard equations, which also appear in TABLE I. We observe that 50% of the mechanical energy is produced within the radial inlet zone and this intense energy exchange is due to the prominent effect of Coriolis forces. We can observe that approximately 80% of the energy transformation takes place upstream of the axial rotor exit zone. We have tested the same point with a greater number of blades (13 blades instead of 11 blades as above). In this case the work per unit mass obtained is equal to 17720,14 J/kg which differs by 3% compared to the previous calculations.

This numerical observation extended to a real fluid simulation explains the technological evolution towards current rotors for which the exit profile is very compact and has a reduced incidence.

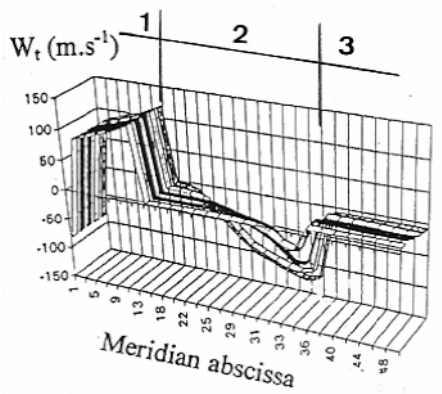

Figure 10. Relative tangential velocities at five lines

TABLE I. LOCAL AND CUMULATED MECHANICAL ENERGY PRODUCTION FROM ROTOR SIMULATION

Mobile rotor	1 *(kJ/kg)*	1+2 *(kJ/kg)*	1+2+3 *(kJ/kg)*
$U_1V_{1t} - U_2V_{2t}$	9 408 53%	13 767 78%	17 761 100%
$U_1W_{1t}-U_2W_{2t}+U_1^2-U_2^2$	9 408 53%	13 767 78%	17 761 100%
$\frac{1}{2}\left[\left(V_1^2-V_2^2\right)+\left(U_1^2-U_2^2\right)-\left(W_1^2-W_2^2\right)\right]$	9 392 53%	13 744 77%	17 758 100%
$\int\frac{dP_i}{\rho}$	9 364 53%	13 768 78%	17 763 100%
$\int dW_a=\int\frac{dP}{\rho}+\int\frac{dV^2}{2}$	9 361 53%	13 731 79%	17 455 100%

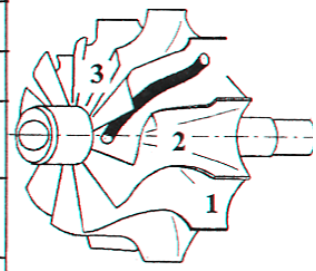

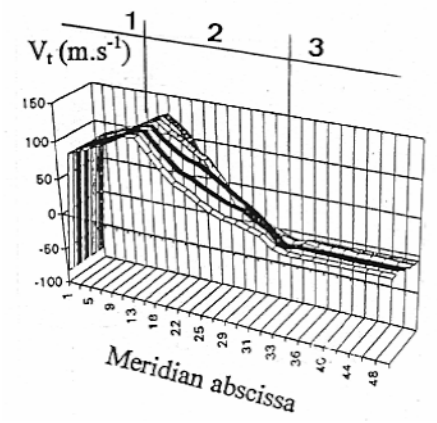

Figure 11. Absolute tangential velocities at five lines

5. 1D Modeling

A complementary analysis of the flow within each sub-block of the turbine helps to take into account the effect of losses and to initialize aero and thermodynamic conditions of the mean flow between inlet and exit to the rotating blades (*Figure 12*). The local blade geometry is so that the shape is supposed to satisfy both centripetal and aerodynamic conditions within the turbine. The gas is assumed perfect and the fluid is considered viscous and compressible. Potential energy is negligible; the turbulent 1D flow is stable on average and adiabatic.

5.1 Dissipative phenomena

The reduced models of losses are derived from the local and the detailed entropic analysis. Okazaki (1992) establishes the model of losses through leakage. Losses by mixing and viscous effects are evaluated by means of models extracted from appropriate articles (Baines 1992, Casartelli et al 1997). We insist in this paper on the incidence losses which undergo a specific entropy analysis since this source of energy dissipation is prominent over a wide running range (Descombes 1997). In the inlet of the rotor, the blade is at a geometrical angle of β*=90°, and the flow trajectory necessarily satisfies the relation $W=W_m$, this condition is imposed by the blade geometry, the relative speed W here being equal to the mean speed W_m. The suffix ‘ refers to the conditions just after the inlet of the rotor, and the enthalpy h’ can be evaluated from either relative equation (6) or rothalpic equation (7) total enthalpy, both of which remain constant at rotor inlet.

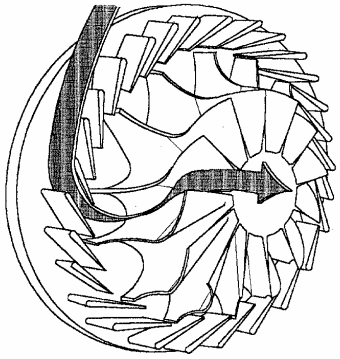

Figure 12. Helicoradial turbine stage

$$h_{iw} = h + \frac{W^2}{2} = h' + \frac{W'^2}{2} \qquad (6)$$

$$h' = I - \frac{W'^2}{2} + \frac{U^2}{2} \qquad (7)$$

5.2 Resolution approach

By combining the equation of momentum and the equation of energy, a complete flow description, in absolute and relative terms can be established, where I and hi represent respectively the total rothalpic enthalpy and total absolute enthalpy. This description complies with equations (8) and (9), established without restrictions on local entropy production in adiabatic flow.

$$I = h + \frac{W^2}{2} - \frac{U^2}{2} \qquad (8)$$

$$h_i = I + UV_\theta \tag{9}$$

The mass balance, relative to sonic conditions within the bladed channel, is expressed by (10), where the subscripts w_1 and w_2 identify the inlet and outlet borders of the rotor in rotational coordinates. A_{*W1} and A_{*W2} represent the associated sonic sections and β_1 and β_2 the incidence angles.

$$A_{*w2}\sin\beta_2 = A_{*w1}\sin\beta_1 \frac{P_{iw2is}}{P_{iw2}}. \left[1+\frac{U_2^2-U_1^2}{2Cp\,T_{iw1}}\right]^{\frac{-(\gamma+1)}{2(\gamma-1)}} \tag{10}$$

The total relative pressure loss is expressed as a function of the calculated increase of the static enthalpy (Equation 11) and of the entropy production (Equation 12). The relative efficiency of the energy transformation within the rotor is given by (13).

$$TdS = dh - \frac{dP}{\rho} \tag{11}$$

$$\int_1^2 \frac{dP}{P} = \frac{\gamma}{\gamma-1}\int_1^2 \frac{dT}{T} - \int_1^2 \frac{dS}{r} \tag{12}$$

$$\eta_w = \frac{P_{iw2}}{P_{iw2is}} \tag{13}$$

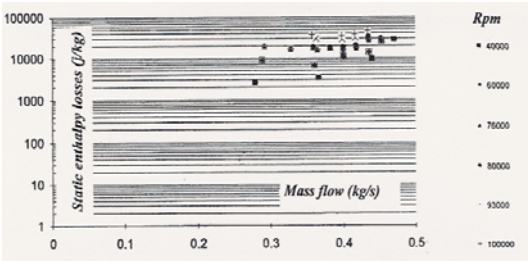

Figure 13. Relative static enthalpy losses within the rotor

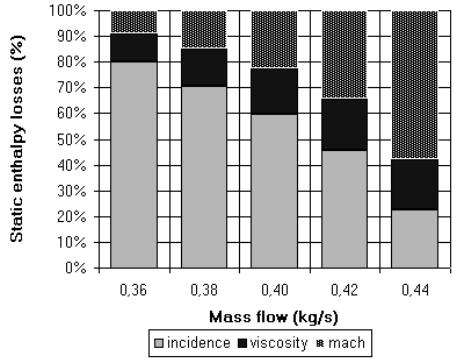

Figure 14. Relative proportions of mean losses within the stage turbine (N = 80000 rpm)

Losses due to the incidence mismatch and to sudden enlargement at the vaned channel outlet are derived from Borda-Carnot and when choking is about to occur, reference is made to work conducted by Pluviose (1991) and Matyshok (1997) who evaluate the losses associated with supersonic jets in the shape of a loss factor (Equation 14), expressed at either side of the shock wave in reference to an ideal transformation.

$$\zeta = 1 - \left[\frac{M_2}{M_{2,is}}\right]^2 \tag{14}$$

5.3 Validation of results

Simulation results undergo a systematic analysis for an 80% open distributor position. Conditions at the turbine inlet are P_{ie}=250000 Pa, T_{ie}=773 K, $0.1<q_m<0.5$ kg.s^{-1}. Losses due to leakage are, in accordance with Spraker (1987), of the order of 4% for a marked negative incidence mismatch and fall progressively to about 1% near the adaptation flow/blade inlet profile.

Figure 13 shows the 1D reduction results of the losses within the rotor as a function of rotor speed. *Figure 14* shows the distribution of incidence, viscosity and compressibility within the rotor as a function of the mass flow at 80,000 rpm. One observes that the distribution of incidence losses at rotor inlet represents a major source of losses over a wide range of mass flow. We can note that for a fixed peripheral velocity U equal to 167 m/s (N_t = 40000 rpm), the relative velocity profiles evolve progressively from negative to positive incidence as a function of the flow rate, whereas for other running points, the relative velocity W always remains at negative incidence.

This reduced 1D model does not make secondary losses appear, which is confirmed by an experimental study (*Figure 15*) led within the laboratory (Lavy et al 1991). The measure on test bed concerns the 2D flow description of the incidence flow profile deviation as a function of the radius position at the outlet rotor (Lavy et al. 1991). This modeling gives also convenient correlation in terms of radial velocity and pressure distributions (Benisek, 1994, Ehrlich, 1997). Connor and Flaxington (1994), Minegishi et al (1995) observe the same trends.

One remarks that most empirical expressions for flow-profile deviation mentioned in articles are often geometrical, and fail to take into account changes in mass flow and the associated incidence variations. Hawthorne (1994) suggests expressing the variation of flow-profile deviation by relating the current exit angle β to

the sonic angle β‘ at the throat and we are working on this point.

This work has contributed to establishment of a complete calculation scheme within each sub-block of a variable geometry turbocharger turbine and thus the permeability characteristics of the machine in relation to the distributor opening position (Descombes, 1998). The complete simulation results have undergone experimental validation on both a turbocharger test bench and a Diesel engine (Descombes, 1997).

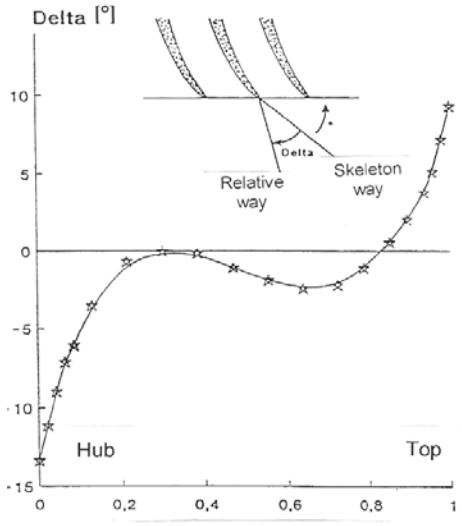

Figure 15. 2D flow measures of the incidence flow profile deviation at the outlet rotor versus reduced radius of the rotor

Calculated results are compared with the experimental performance map. The analysis is conducted over the 60000 < N_t(rpm) < 80000 rotor speed range. The error in efficiency values is approximately 5% for expansion ratios in the range 1.25< τ <1.4. The analysis is conducted for a specific experimental rotor speed line, 2769 (77000) which falls between the simulated lines 2734 (76000) and 2877 (80000) for an 80% open distributor position. The 2734 (76000) model speed profile is very similar to the experimental 2769 (77000) profile (*Figure 16*).

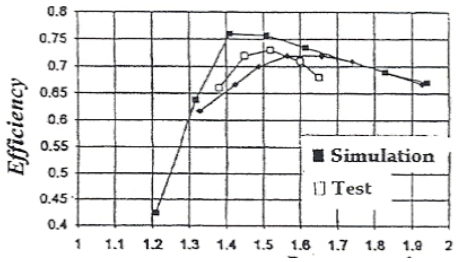

Figure 16. Efficiency versus expansion ratio

Simulation results cover a widened expansion ratio range 1.2<τ<1.9 compared to experimental values, for 1.4<τ<1.65. The average difference remains less than 3%, while the maximum difference is around 6%. We note a small translation of the efficiency curve for the 2877 (80000) curve as a function of the expansion ratio. However, we observe a deviation of specific mass flow rate, the simulation giving values 6% higher with respect to the considered point (Descombes, 1997).

6. Conclusion

Detailed results of the energy transformation within a turbine stage as a function of flow conditions at its inlet have been presented in this paper. A multi-dimensional analysis has highlighted the variability of the local distribution of velocities and pressures within the rotor and gives a real image of energy transformation for nearly ideal zero incidence conditions at the rotor inlet. The permeability characteristics within the rotor and an entropy analysis enabled via models reduction have shown that flow/blade profile mismatch remains very prominent over a wide running range in such small machinery. The simulation results have been compared with the experimental results conducted on specific turbocharger test bench. This study has contributed to the construction of a complete scheme validated on a turbocharger and truck engine test bench within a variable geometry turbocharger.

Nomenclature

F	stress torque
h	static enthalpy
I	rothalpy
M	Mach number
M	momentum torque
N_T	speed turbine
P	static pressure
P_i	total pressure
q_m	mass flow
r	radius rotor
S	entropy
T_i	total temperature
v	elementary volume
β	rotor blade inlet angle geometry
β’	rotor blade exit angle geometry
τ	expansion ratio

Subscripts

i	total
m	meridian
w	relative coordinates
1	surface S_1
2	surface S_2

References

Baines, N. C., 1992, “Introduction to radial turbine technology” V. K. I., Lecture Series 9205.

Benisek, E., 1994, "Comparisons of laser and pneumatic measurements in a turbocharger turbine", *I MechE* 1994, C484/018.

Casartelli, E., Saxer, A.P., Gyarmarthy, G., 1997, "Numerical flow analysis in a subsonic vaned radial diffuser with leading edge redesign" *Asme paper* GT97.

Connor, W.A., Flaxington, 1994, "A one dimensional performance prediction method for radial inflow turbine" *ImechE* 1994, C405/017.

Descombes, G., 1997, "Contribution à l'étude des performances d'une turbine de suralimentation à géométrie variable" Doctoral thesis of University Paris 6, 1997.

Descombes, G., Duan, Q., Jullien, J.,Parkinson, N., 1998, "Study of the performance of a variable geometry turbocharger", 22nd CIMAC, session no 10.08, Copenhaguen, may 1998.

Ehrlich, D.A., Lawless, P.B. and Fleeter, S., 1997, "Particle image velocimetry characterization of a turbocharger turbine inlet flow" *SAE Paper* 970343.

Hawthorne, W.R., 1994, *Aspects of the characteristics of radial flow turbines*, Institution of Mechanical engineers, C 484/004, 1994.

Lavy, J., Duan, Q., Jullien, J., Bois, G., 1991, "Mesure des caractéristiques de fonctionnement de turbines de turbocompresseurs en régimes stationnaire et pulsé", Revue française de mécanique, 1991-3.

Matyshok, B., Stoffel, B., 1997, "Experimental investigations of the flow at the rotor oulet of a turbocharger turbine", *2nd European conference on turbomachinery*, Antwerpen, March 5-7, 1997.

Minegishi, H., Matsushita, H., Sakakida, M., 1995, "Development of a small mixed flow turbine for automotive turbochargers", *Asme paper* 95GT53.

Okazaki, Y., 1992, "Development of variable area radial turbine for small turbochargers" *Asme Paper* GT 92.

Pluviose, M., 1991, "Instabilities of flow in sudden enlargement" *Asme*,Vol. 128, H00706.

Spraker, N., 1987, "Contour clearance loss in radial inflow turbines for turbocharger" *Asme Paper* 87ICE52.

Toussaint, M., Descombes, G., Pluviose, M., 1999, "Research into variable geometry turbochargers without wastegates", Institution of Mechanical Engineers, *3rd European conference transactions on turbomachinery, fluid dynamics and thermodynamics*, 2-5 march 1999, London, *ImechE Paper*, pp. 883-891, ISSN 1356-1448.

Wu, C.H., 1951, "A general through flow theory of fluid flow with subsonic or supersonic velocity in turbomachines having arbitrary huts and casing shapes" Nasa T2388, 1951.

Zangeneh, M., 1988, "Three dimensional flow in radial inflow turbines" *Asme paper* 88GT103.